Large scale arrays of four-state vortex domains in $BiFeO_3$ thin film

W. Y. Wang, Y. L. Zhu, Y. L. Tang, Y. B. Xu, Y. Liu, S. Li, S. R. Zhang, Y. J. Wang, and X. L. Ma

Citation: Appl. Phys. Lett. **109**, 202904 (2016); doi: 10.1063/1.4967878
View online: http://dx.doi.org/10.1063/1.4967878
View Table of Contents: http://aip.scitation.org/toc/apl/109/20
Published by the American Institute of Physics

Large scale arrays of four-state vortex domains in $BiFeO_3$ thin film

W. Y. Wang,[1,2] Y. L. Zhu,[1,a)] Y. L. Tang,[1] Y. B. Xu,[1] Y. Liu,[1] S. Li,[1] S. R. Zhang,[1] Y. J. Wang,[1] and X. L. Ma[1]

[1]*Shenyang National Laboratory for Materials Science, Institute of Metal Research, Chinese Academy of Sciences, Wenhua Road 72, 110016 Shenyang, China*

[2]*Science and Technology on Surface Physics and Chemistry Laboratory, 621908 Jiangyou, Sichuan, China*

(Received 23 August 2016; accepted 29 October 2016; published online 15 November 2016)

Exotic domain states, like vortex, offer the promise of superior properties and the potential disclination strain is a key factor for their formation in ferroelectrics. Here we show that large scale arrays of four-state vortex domains can be obtained in rhombohedral $BiFeO_3$ thin films grown on $PrScO_3$ substrates by pulsed laser deposition. Cs-corrected scanning transmission electron microscopy demonstrates that each vortex domain is comprised of four ferroelectric variants with two 180° domain walls and two 109° domain walls. Atomic mappings of the lattice distortions unit cell by unit cell reveal that the cores of the vortex might be charged. The strains are mainly concentrated on domain walls. The formation mechanism of such large scale vortex-like states was discussed. *Published by AIP Publishing*. [http://dx.doi.org/10.1063/1.4967878]

Topological defects,[1] such as domain walls and exotic domain states in ferroics, are typical features of ordered materials and have long been of interest in the field of solid state physics.[1–3] One of the typical topological defects is vortex, of which the order parameter features a curling fashion with the possibility of special physical characteristics existing at the cores.[4,5] The ability to control both the arrangement and the amount of these topological defects could be of importance for related studies and potential applications.[6,7]

In fact, the final domain state rests with the competition between various energies associated to exchange and crystallographic anisotropy of ferroics.[3,8,9] For ferromagnetics, Kittel in the 1950s pointed out the influence of crystallographic anisotropy on magnetic domain patterns where vortex states could exist in systems with small anisotropy.[8,9] Subsequent research has thoroughly demonstrated the existence of ferromagnetic vortex structures through experiments.[5,10,11] However, for ferroelectric materials such as $Pb(Zr)TiO_3$ and $BaTiO_3$, the coupling between polarization and lattice might be so strong that the disclination strain at the area of vortex can be as high as 25%, far beyond their plastic deformation limits.[12] In addition, such disclination strain diverges with the geometric size of a system. Thus, vortex related states in ferroelectrics were often observed under certain circumstances, for example, in disk-shaped nano capacitors,[13,14] nano dots[15,16] and nano sheets, etc.[17,18]

As practical devices are mainly based on thin films, manipulation of the geometry of the vortex related exotic domain states in thin films is valuable for further studies and applications of the exotic domain states. For ferroelectric thin films, several studies indeed demonstrated the existence of as-grown vortex states. Jia *et al*. pointed out a flux-closure dipole state existing at the intersection of the 180° domain wall and heterointerfaces with insufficient screening quality.[19] A similar situation also exists in 109° domain patterned $BiFeO_3$ (BFO) thin films, where nano, four-quadrant vortex (FQV) states were found near insulating heterointerfaces.[20] Recently, Tang *et al*.[12] and Yadav *et al*.[21] both found full flux closure vortex domains in $PbTiO_3$ multilayer films. In addition to the cross-sectional domain patterns, in-plane vortex domains are also essential to study for their physical properties especially at the core area, for example, with scanning probe microscope (SPM) based techniques.[4,22]

Here we show that large-scale self-organized arrays of in-plane four quadrant vortex (FQV) states can be obtained in BFO thin films. Using advanced aberration-corrected transmission electron microscopy, the detailed atomic structural features of these in-plane FQV states in BFO thin film on $PrScO_3$ (PSO) substrate were studied. The results show that lattice distortions are mainly concentrated at domain walls, which is an indication of the small disclination strains of such FQV states. The present study would benefit the related studies on vortex-like domain states in ferroelectrics.

BFO thin films (~55 nm) were grown on orthorhombic (110) PSO single crystal substrates by pulsed laser deposition (PLD).[23] At room temperature, bulk BFO has a rhombohedral structure ($a = 3.965$ Å, $\alpha = 89.4°$) with spontaneous polarization (***Ps***) in the ⟨111⟩ direction, and it contains eight ferroelectric variants corresponding to four ferroelastic variants. For BFO grown on orthorhombic (o) scandate substrate, the four ferroelastic variants degenerate into two, where a stripe domain pattern can readily be obtained.[24,25] Here, for simplification, the rhombohedral BFO is treated as a pseudocubic (pc) structure. Fig. 1(a) displays a typical domain pattern morphology of a cross-sectional BFO thin film (~55 nm) grown on PSO. The image is recorded far away from the $[-110]_o$ zone axis of PSO under a two-beam condition. The subscripts o and pc represent orthorhombic and pseudocubic, respectively. A stripe domain pattern with domain walls on $(010)_O$ planes (dotted blue lines) can be clearly identified. On one hand, the (110) orientated scandates with a space group of Pbnm have a monoclinic distorted constrain onto BFO which can reduce the four ferroelastic variants of BFO into two, resulting in stripe-like domain patterns.[25,26] It is the typical feature of a mechanical boundary condition that influences the domain pattern geometry. On the other hand, the scandate

a)Electronic mail: ylzhu@imr.ac.cn

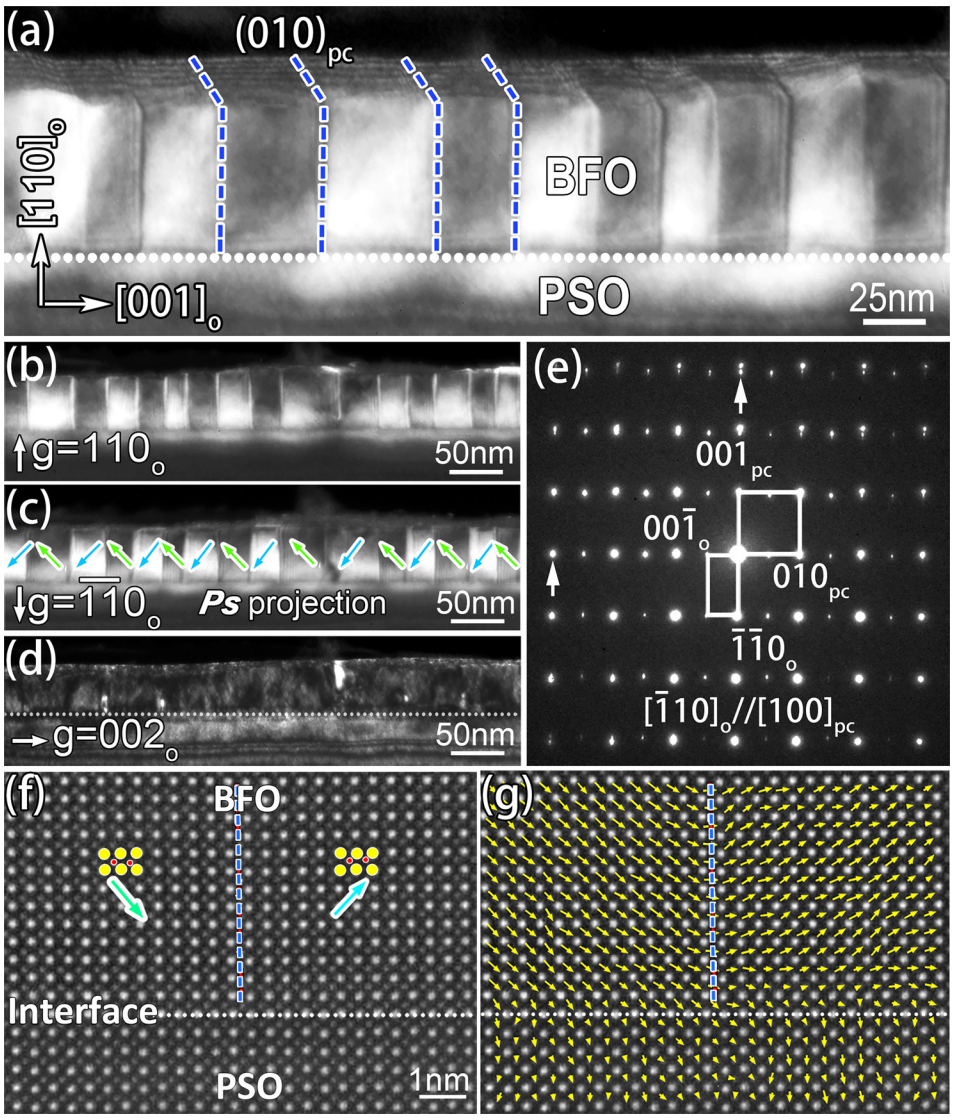

FIG. 1. (a) A typical dark field image showing the domain pattern of a 55 nm thick BFO film on orthorhombic PSO substrate. (b)–(d) Two-beam dark field images showing the domain patterns of a large area using different reflections: $g=(110)_o$, $g=(-1-10)_o$, $g=(002)_o$, respectively. The deduced ***Ps*** projections are noted by arrows. (e) A selected area electron diffraction pattern taken from the area containing both BFO film and PSO substrate along the $[-110]_o$ zone axis. (f) An atomic resolution HAADF-STEM image of cross-sectional BFO/PSO thin film showing the 109° domain pattern. The yellow circles denote Bi atoms while red circles denote Fe atoms. Arrows denote the directions of Fe sub-lattice displacement. (g) The superposition of the atomic mapping with the Fe displacement vectors, showing the polarizations across the 109° domain wall of Figure (f).

substrates are insulators, so the electrical boundary condition for BFO thin films is open circuit. The polarization directions of nearby domains in a domain pattern prefer to show a "head to tail" configuration near the film/substrate interface to reduce the depolarization field. As a result, BFO thin film develops a 109° polarization configuration.[24,26] In TEM experimental observation, the polarization vector direction of each domain can be deduced by making use of the failure of Friedel's law,[27,28] where images give rise to bright contrast for the domain with the corresponding polarization (***Ps***) vector satisfying $\mathbf{g}\cdot\boldsymbol{Ps}>\mathbf{0}$. Figs. 1(b)–1(d) are two-beam dark field images using different reflections of $g=(110)_o$, $g=(-1-10)_o$, and $g=(002)_o$, respectively, clarifying the ***Ps*** projection arrangement (labeled by colored arrows). For the stripe-like 109° domains, the periodic up and down arrangement of the out-of-plane ***Ps*** components can reduce the out-of-plane depolarization field introduced by the insulated substrate.[20,29] In addition, such an incorporation of mechanical and electrical boundary conditions can indeed generate interesting in-plane domain patterns which are presented in the following context. To judge the quality of the thin film system, electron diffraction experiments were carried out. Fig. 1(e) is a superposed selected area electron diffraction pattern taken from the area containing both BFO film and PSO substrate along $[-110]_o$ the zone axis. A definite epitaxial relationship can be determined to be $[-110]_o//[100]_{pc}$ and $(001)_o//(010)_{pc}$. The spot splitting along the $[001]_{pc}$ direction denoted by vertical arrow can be identified which is due to the difference in out-of-plane lattice parameters of BFO and PSO. It is noted that the in-plane lattice parameters keep the same since no spot splitting can be observed. In order to clearly reveal the 109° domain pattern, an atomically resolved high angle angular dark field (HAADF)-scanning transmission electron microscopy (STEM) image in the cross-sectional BFO/PSO thin film is shown in Fig. 1(f), where the yellow circles denote Bi atoms while red circles denote Fe atoms, and the arrows denote the directions of Fe sub-lattice displacements. The superposition of the atomic mapping with the Fe displacement vectors is displayed in Fig. 1(g), showing the polarization distribution across the 109° domain wall.

The in-plane domain pattern of the BFO thin film is revealed in Figs. 2(a)–2(c). In Fig. 2(a), the long stripe-like domains with bright and dark contrasts alternately arranged along $[001]_o$ ($[010]_{pc}$) direction are believed to be 109° domains (the domain walls are noted by dashed blue lines),

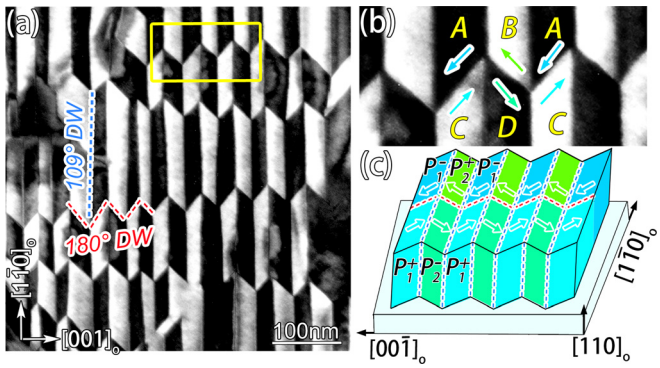

FIG. 2. (a) A dark field image showing in-plane domain patterns obtained near the $[110]_o$ ($[001]_{pc}$) zone axis. (b) An enlarged area outlined by a yellow frame in (a) with the proposed ferroelectric variants (A, B, C, D). The polarization projections are labeled by arrows. Each FQV state is comprised by four intersecting ferroelectric variants (A–D). (c) A stereo schematic showing the in-plane FQV structures. Arrows denote the directions of ***Ps*** projections.

while the zigzag domain walls (dashed red lines) along $[1\text{-}11]_o$ ($[\text{-}110]_{pc}$) and $[\text{-}111]_o$ ($[110]_{pc}$) directions intersecting with these 109° domains were also observed. Based on the phenomenological theory of domain wall geometry proposed by Speck,[30] these zigzag domain walls should belong to 180° type. The universal formation of the 180° domain walls is expected to reduce the in-plane depolarization effects. It is of special interest to notice that the intersection of these 109° and 180° domain walls in Fig. 2(a) in fact represents a kind of exotic domain array, namely, FQV arrays, as shown in Fig. 2(b). Each FQV includes four nearby parallelogram shaped domains, for example, A-B-C-D. Such a kind of domain pattern is quite similar to the vortex domains where four nearby domains comprise clockwise or anti-clockwise polarization configurations.[12] The geometry of the in-plane FQV array is also schematically depicted in Fig. 2(c) where the ferroelectric variants arrangement and the corresponding ***Ps*** projections are indicated.

To further confirm this point, as shown in Fig. 1(f), we again performed an aberration-corrected scanning transmission electron microscopy (STEM) which has been widely used to study complex oxides, especially perovskite ferroelectrics.[23,31] Figs. 3(a) and 3(b) are atomic resolved HAADF-STEM images of two typical FQV states. There are four domains A-D and four corresponding domain walls. The determination of these domains is based on the directions of sub-lattice Fe displacements, where the ***Ps*** projection is opposite to sub-lattice displacement.[12,20,23] The polarization relation between the nearby quadrant domains of each FQV can then be easily identified. The ***Ps*** arrangements from domain A to domain B (A/B) and from domain C to domain D (C/D) are both "head-to-tail," while the ***Ps*** arrangements from domain A to domain C (A/C) and from domain B to domain D (B/D) are antiparallel. This kind of ***Ps*** arrangement features an important fingerprint for identifying the domain wall types. Likewise, according to the structural distortions, the domain walls of A/B and C/D are $(010)_{pc}$ indicated by dashed blue lines in Figs. 3(c) and 3(d); the domain wall of A/C is $(110)_{pc}$ while the domain wall of

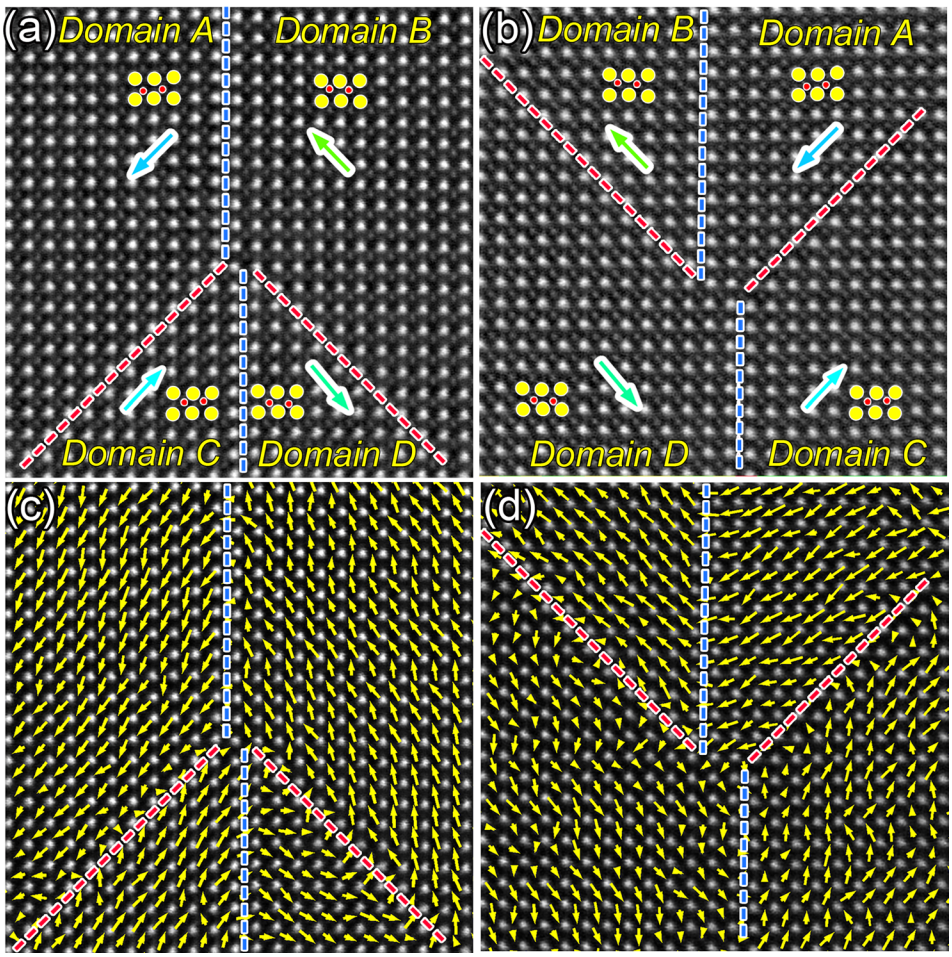

FIG. 3. ((a) and (b)) Atomic resolved HAADF images of two kinds of FQV states. The yellow circles denote Bi atoms while red circles denote Fe atoms. 109° domain walls are noted by dotted blue lines and 180° domain walls are noted by dotted red lines. Arrows show the direction of the displacement vectors, which is opposite to the direction of polarization projections. ((c) and (d)) Two dimensional mappings of the displacement vectors of Fe sub-lattice.

B/D is $(1\text{-}10)_{pc}$ (red dashed lines). As pointed out by previous theoretical and experimental works, it is found that the 109° domain wall has a "head-to-tail" ***Ps*** configuration with domain walls on {100} planes, while the 180° domain wall has an anti-parallel ***Ps*** configuration with domain walls on {110} planes.[24,30] Thus domains A/B and C/D form 109° domains while domains A/C and B/D form 180° domains. This configuration of the FQV matches well with inspections based on the contrast analysis as shown in Figs. 1 and 2. The interesting feature of such an FQV state can be further revealed by two dimensional mappings of the sub-lattice displacement vector, which can reflect the ***Ps*** arrangement. In a unit cell by unit cell inspection, the vortex-like Fe sub-lattice displacement distribution can be readily observed in Figs. 3(c) and 3(d), in which the displacement vectors are relatively uniform in each domain, while reorientations exist at domain walls. The overall displacement vectors form a pattern which is similar to the vortex states described in Ref. 20. It is worthwhile to point out that the vortex domains are several nanometers in size near the interface, which is believed to be related to the influences of the substrate in Ref. 20.

It is generally believed that vortex-related states would introduce huge local disclination strains where severe lattice distortions are expected.[12] For the FQV states in the present study, the uniform distribution (Fig. 2(a)) in an in-plane fashion implies that the additional strain caused by a domain intersection would not be prominent. To demonstrate the internal strain for such an FQV state, we quantitatively analyze the local lattice distortions using line profiles (the results are not shown here) and 2-D mappings of the lattice distortions. The 2-D mappings of the lattice distortions are suitable to show the distribution of the lattice distortion. To better display the strain state of the FQV, we convert the lattice spacing changes into horizontal strain ε_{xx} and vertical strain ε_{yy} ($\varepsilon_{xx} = \frac{Lx-Ref.}{Ref.} \times 100\%$, $\varepsilon_{yy} = \frac{Ly-Ref.}{Ref.} \times 100\%$, here *Ref.* is 4.0 Å, ε_{xx} represents the relative changes of lattice spacing *Lx*, while ε_{yy} represents the relative changes of lattice spacing *Ly*), and in the meanwhile we also extract the lattice rotations *Rx* and *Ry*, representing the rotation angles of horizontal lattice and vertical lattice, respectively, as shown in Fig. 4. It is obvious that the remarkable changes of both the lattice spacing and the lattice rotation appear basically at the domain walls. Considering the intrinsic lattice distortions of the 180° and 109° domain walls,[23,32] these lattice distortions mainly originate from the domain walls, and additional discernable lattice distortion can hardly be found in the domain matrix. This indicates that the disclination strain for such an FQV is relatively small, which is different from the giant disclination strain in tetragonal ferroelectrics.[12]

In spite of the obvious lattice distortions at the domain walls, structures at the core area are interesting since the core might involve a charged domain wall (Fig. 3(b)). The presence of a charged domain wall usually induces unusual structural distortions[20,23] and exotic physical properties. Balke *et al.* showed that the conducting behavior was enhanced at the vortex core in BFO.[4] Efforts will be made to further reveal the details of such a charged FQV core in the future.

For the formation of specific domain states, two aspects can be taken into account. One is the thin film growth rate, which has been demonstrated to have an important influence on the geometries of BFO domain states. Martin *et al.* showed that mosaic-like domains were observed with high growth rates (~1–2 Å/s); while at low growth rates (~0.1–0.3 Å/s), a stripe-like domain state could be obtained.[33] For the present BFO thin film, the growth rate is close to the low growth rates. The stripe-like domains are in good agreement with the

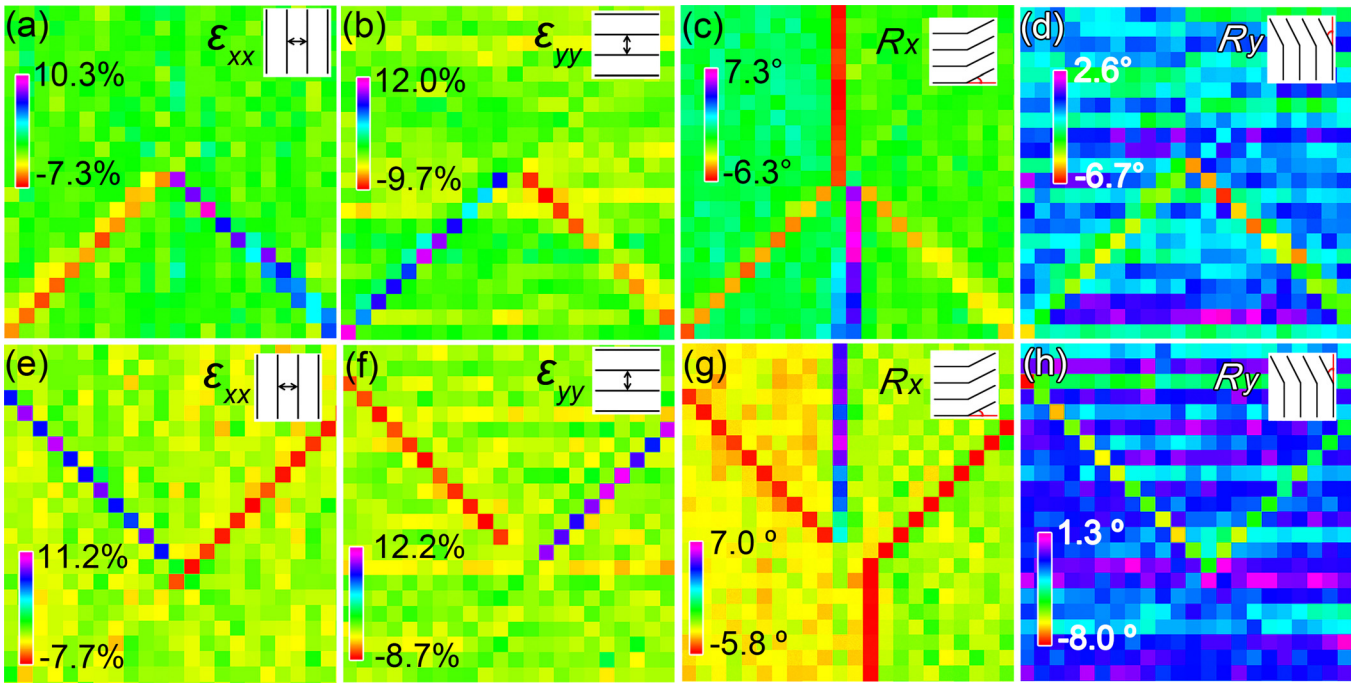

FIG. 4. 2-D mappings of the horizontal strain ε_{xx} (a), vertical strain ε_{yy} (b), horizontal lattice rotation *Rx* (c) and vertical lattice rotation *Ry* (d), respectively, for the vortex domains shown in Fig. 3(a). (e)–(h) are 2-D mappings of ε_{xx}, ε_{yy}, *Rx*, and *Ry*, corresponding to the vortex domains shown in Fig. 3(b). Note that remarkable changes of lattice spacing and lattice rotation occur at the domain walls.

phenomenological theory which predicts the domain geometries under an equilibrium state. Another key aspect that determines the domain pattern geometries is substrate-induced strains. Under a large tensile strain,[29,34] BFO would possess a structural distortion where the polarization vector would tilt from the body diagonal [111] of prototypical rhombohedral BFO into the in-plane direction.[29] Such a rotation of the ***Ps*** vector would of course result in the in-plane component of ***Ps*** being larger than that of the out-of-plane component and increase the ratio of in-plane depolarization field which would account for the multiple in-plane domain configurations.

For each FQV, 109° ferroelastic domains are interrupted by 180° ferroelectric domains, and the introduction of more ferroelectric domain walls does not result in a large disclination strain. The intrinsic lattice distortion around the 180° domain wall of BFO is small compared to the disclination strain in 90° ferroelastic domains in tetragonal ferroelectrics. Large disclination strains are expected to develop if a domain pattern is comprised of purely ferroelastic domains, whereas small disclination strains would be possible if it contains ferroelectric domains.

In conclusion, we demonstrated large scale arrays of in-plane four-state vortex domains in strained BFO thin films and quantitatively analyzed the atomic structures using advanced aberration corrected transmission electron microscopy. Such exotic domain patterns are comprised of two 180° and two 109° domain walls, and lattice distortion mappings reveal that disclination strains are not eminent in spite of the domain wall lattice distortion. These findings provide further insights in exploring the in-plane vortex structures for future studies and possible applications.

This work is supported by the National Natural Science Foundation of China (Nos. 51231007, 51571197, 51501194, 51671194, and 51521091), National Basic Research Program of China (2014CB921002), and the Key Research Program of Frontier Sciences, CAS (QYZDJ-SSW-JSC010). Y. L.T. acknowledges the IMR SYNL-T.S. Kê Research Fellowship and the Youth Innovation Promotion Association CAS (No. 2016177).

[1]N. Mermin, Rev. Mod. Phys. **51**, 591 (1979).
[2]G. Catalan, J. Seidel, R. Ramesh, and J. F. Scott, Rev. Mod. Phys. **84**, 119 (2012).
[3]J. M. Gregg, Ferroelectrics **433**, 74 (2012).
[4]N. Balke, B. Winchester, W. Ren, Y. H. Chu, A. N. Morozovska, E. A. Eliseev, M. Huijben, R. K. Vasudevan, P. Maksymovych, J. Britson, S. Jesse, I. Kornev, R. Ramesh, L. Bellaiche, L. Q. Chen, and S. V. Kalinin, Nat. Phys. **8**, 81 (2011).
[5]A. Wachowiak, J. Wiebe, M. Bode, O. Pietzsch, M. Morgenstern, and R. Wiesendanger, Science **298**, 577 (2002).
[6]D. B. Li and D. A. Bonnell, Annu. Rev. Mater. Res. **38**, 351 (2008).
[7]L. Feigl, P. Yudin, I. Stolichnov, T. Sluka, K. Shapovalov, M. Mtebwa, C. S. Sandu, X. K. Wei, A. K. Tagantsev, and N. Setter, Nat. Commun. **5**, 4677 (2014).
[8]C. Kittel, Phys. Rev. **70**, 965 (1946).
[9]C. Kittel, Rev. Mod. Phys. **21**, 541 (1949).
[10]K. Runge, Y. Nozaki, Y. Otani, H. Miyajima, B. Pannetier, T. Matsuda, and A. Tonomura, J. Appl. Phys. **79**, 5075 (1996).
[11]R. J. Harrison, R. E. Dunin-Borkowski, and A. Putnis, PNAS **99**, 16556 (2002).
[12]Y. L. Tang, Y. L. Zhu, X. L. Ma, A. Y. Borisevich, A. N. Morozovska, E. A. Eliseev, W. Y. Wang, Y. J. Wang, Y. B. Xu, Z. D. Zhang, and S. J. Pennycook, Science **348**, 547 (2015).
[13]A. Gruverman, D. Wu, H. J. Fan, I. Vrejoiu, M. Alexe, R. J. Harrison, and J. F. Scott, J. Phys. Condens. Matter **20**, 342201 (2008).
[14]B. J. Rodriguez, X. S. Gao, L. F. Liu, W. Lee, I. I. Naumov, A. M. Bratkovsky, D. Hesse, and M. Alexe, Nano Lett. **9**, 1127 (2009).
[15]A. Schilling, D. Byrne, G. Catalan, K. G. Webber, Y. A. Genenko, G. S. Wu, J. F. Scott, and J. M. Gregg, Nano Lett. **9**, 3359 (2009).
[16]A. Schilling, S. Prosandeev, R. G. P. McQuaid, L. Bellaiche, J. F. Scott, and J. M. Gregg, Phys. Rev. B **84**, 064110 (2011).
[17]R. G. McQuaid, L. J. McGilly, P. Sharma, A. Gruverman, and J. M. Gregg, Nat. Commun. **2**, 404 (2011).
[18]R. G. McQuaid, A. Gruverman, J. F. Scott, and J. M. Gregg, Nano Lett. **14**, 4230 (2014).
[19]C. L. Jia, K. W. Urban, M. Alexe, D. Hesse, and I. Vrejoiu, Science **331**, 1420 (2011).
[20]C. T. Nelson, B. Winchester, Y. Zhang, S. J. Kim, A. Melville, C. Adamo, C. M. Folkman, S.-H. Baek, C.-B. Eom, D. G. Schlom, L. Q. Chen, and X. Pan, Nano Lett. **11**, 828 (2011).
[21]A. K. Yadav, C. T. Nelson, S. L. Hsu, Z. Hong, J. D. Clarkson, C. M. Schlepütz, A. R. Damodaran, P. Shafer, E. Arenholz, L. R. Dedon, D. Chen, A. Vishwanath, A. M. Minor, L. Q. Chen, J. F. Scott, L. W. Martin, and R. Ramesh, Nature **530**, 198 (2016).
[22]J. Seidel, L. W. Martin, Q. He, Q. Zhan, Y. H. Chu, A. Rother, M. E. Hawkridge, P. Maksymovych, P. Yu, M. Gajek, N. Balke, S. V. Kalinin, S. Gemming, F. Wang, G. Catalan, J. F. Scott, N. A. Spaldin, J. Orenstein, and R. Ramesh, Nat. Mater. **8**, 229 (2009).
[23]W. Y. Wang, Y. L. Tang, Y. L. Zhu, Y. B. Xu, Y. Liu, Y. J. Wang, S. Jagadeesh, and X. L. Ma, Adv. Mater. Interfaces **2**, 1500024 (2015).
[24]Y. H. Chu, Q. Zhan, L. W. Martin, M. P. Cruz, P. L. Yang, G. W. Pabst, F. Zavaliche, S. Y. Yang, J. X. Zhang, L. Q. Chen, D. G. Schlom, I. N. Lin, T. B. Wu, and R. Ramesh, Adv. Mater. **18**, 2307 (2006).
[25]Y. H. Chu, Q. He, C. H. Yang, P. Yu, L. W. Martin, P. Shafer, and R. Ramesh, Nano Lett. **9**, 1726 (2009).
[26]Z. H. Chen, A. R. Damodaran, R. Xu, S. Lee, and L. W. Martin, Appl. Phys. Lett. **104**, 182908 (2014).
[27]M. Tanaka and G. Honjo, J. Phys. Soc. Jpn. **19**, 954 (1964).
[28]T. Asada and Y. Koyama, Phys. Rev. B **70**, 104105 (2004).
[29]Z. Chen, Y. Qi, L. You, P. Yang, C. W. Huang, J. Wang, T. Sritharan, and L. Chen, Phys. Rev. B **88**, 054114 (2013).
[30]S. K. Streiffer, C. B. Parker, A. E. Romanov, M. J. Lefevre, L. Zhao, J. S. Speck, W. Pompe, C. M. Foster, and G. R. Bai, J. Appl. Phys. **83**, 2742 (1998).
[31]Y. L. Tang, Y. L. Zhu, Y. J. Wang, W. Y. Wang, Y. B. Xu, W. J. Ren, Z. D. Zhang, and X. L. Ma, Sci. Rep. **4**, 4115 (2014).
[32]Y. Wang, C. Nelson, A. Melville, B. Winchester, S. Shang, Z.-K. Liu, D. G. Schlom, X. Pan, and L. Q. Chen, Phys. Rev. Lett. **110**, 267601 (2013).
[33]L. W. Martin, Y. H. Chu, M. B. Holcomb, M. Huijben, P. Yu, S. J. Han, D. Lee, S. X. Wang, and R. Ramesh, Nano Lett. **8**, 2050 (2008).
[34]J. C. Yang, Q. He, S. J. Suresha, C. Y. Kuo, C. Y. Peng, R. C. Haislmaier, M. A. Motyka, G. Sheng, C. Adamo, H. J. Lin, Z. Hu, L. Chang, L. H. Tjeng, E. Arenholz, N. J. Podraza, M. Bernhagen, R. Uecker, D. G. Schlom, V. Gopalan, L. Q. Chen, C. T. Chen, R. Ramesh, and Y. H. Chu, Phys. Rev. Lett. **109**, 247606 (2012).